

Geophysical Research Letters[®]



RESEARCH LETTER

10.1029/2022GL102480

Key Points:

- We combine Interferometric Synthetic Aperture Radar and Global Positioning System data to survey the Central Andean volcanoes, some of which have been updated for the first time in over 10 years
- We show the first detection of unrest at Socompa volcano with steady uplift up to 17.5 mm/yr since November 2019
- Deformation patterns are consistent with an ellipsoidal source, stretching from 2.1 to 10.5 km and with a volume change of $\sim 6.2 \times 10^6 \text{ m}^3/\text{yr}$

Supporting Information:

Supporting Information may be found in the online version of this article.

Correspondence to:

F. Liu,
cefl@leeds.ac.uk

Citation:

Liu, F., Elliott, J. R., Ebmeier, S. K., Craig, T. J., Hooper, A., Novoa Lizama, C., & Delgado, F. (2023). First onset of unrest captured at Socompa: A recent geodetic survey at Central Andean volcanoes in Northern Chile. *Geophysical Research Letters*, 50, e2022GL102480. <https://doi.org/10.1029/2022GL102480>

Received 8 DEC 2022
Accepted 26 APR 2023

First Onset of Unrest Captured at Socompa: A Recent Geodetic Survey at Central Andean Volcanoes in Northern Chile

F. Liu¹ , J. R. Elliott¹ , S. K. Ebmeier¹ , T. J. Craig¹ , A. Hooper¹ , C. Novoa Lizama¹, and F. Delgado² 

¹COMET, School of Earth and Environment, University of Leeds, Leeds, UK, ²Department of Geology, Centro de Excelencia en Geotermia Andina, Universidad de Chile, Santiago, Chile

Abstract We report the first detection of unrest at Socompa volcano during our recent survey of Central Andean volcanoes in Northern Chile using Interferometric Synthetic Aperture Radar measurements spanning January 2018 to October 2021. We find that Socompa volcano, whilst initially undeforming and no recorded eruptions for 7.2 kyr, shows a steady uplift (17.5 mm/yr) from November 2019, independently recorded by near-field continuous Global Positioning System data. The deformation pattern can be fitted with pressure increase in an ellipsoidal source region stretching from 2.1 to 10.5 km, with a volume change rate of $\sim 6.2 \times 10^6 \text{ m}^3/\text{yr}$. Our observations of the onset of uplift suggest it is unlikely that a nearby M_w 6.8 deep intraslab earthquake on 3 June 2020 triggered the unrest. The deformation signal we detect indicates the initiation of unrest at Socompa, after at least two decades without measurable deformation, and many thousands of years without volcanic activity.

Plain Language Summary Here we report the first observation of unrest of the Socompa volcano, Northern Chile, which is thought to have last erupted thousands of years ago. Using radar interferometry technique and differencing radar images from two dates, it is possible to retrieve millimeter-level surface displacements during this period. Here, we use a time series of multiple images spanning January 2018 to January 2023, over the Central Andean volcanoes in Northern Chile, to estimate the change in ground movement through time. Combined with Global Positioning System data, we find Socompa volcano started to uplift in November 2019 at a relatively stable speed (of 17.5 mm/yr) without any trace of slowing down up to December 2021. Our analysis suggests that this volcanic deformation is unlikely to have been triggered by a nearby 112 km depth, M_w 6.8 earthquake, which occurred in June 2020, and was thus after the onset time. Deformation at Socompa has similarities with other volcanoes in the Central Andes, where low rates of magmatic uplift have been detected at other apparently quiescent volcanoes. Such large-scale monitoring efforts using remote sensing data are important, as we can better understand the deformation style of these volcanoes in areas that are poorly instrumented.

1. Introduction

Satellite Interferometric Synthetic Aperture Radar (InSAR) measures the Earth's surface deformation at the millimeter-level and has increased the number of volcanoes where deformation has been studied by an order of magnitude (e.g., Biggs et al., 2014; Ebmeier et al., 2018; Poland & Zebker, 2022). InSAR can capture deformation caused by the movement of magma through the Earth's crust (e.g., Reath et al., 2019), by pressure changes within a zone of magma storage (e.g., Chaussard & Amelung, 2012) or overlying hydrothermal system (e.g., Yunjun et al., 2021). In Northern Chile (17.5–27°S), where only 10 of the region's 42 Holocene volcanoes are currently actively monitored using ground-based instrumentation (Aguilera et al., 2022), the systematic displacement measurements possible with InSAR can provide the best record of timings of recent unrest and magmatic activity at Central Andean volcanoes (e.g., Henderson & Pritchard, 2013; Pritchard & Simons, 2004a).

Survey-mode InSAR first detected magmatic deformation in the Central Andes at Uturunco, Lazufre, Cerro Blanco, and Sabancaya-Hualca Hualca in the 1990s (MacQueen et al., 2020; Pritchard & Simons, 2002). Uturunco has been the subject of numerous subsequent studies (e.g., Barone et al., 2019; Fialko & Pearse, 2012; Henderson & Pritchard, 2013; Henderson & Pritchard, 2017; Hickey et al., 2013), showing a reservoir depth of 15–30 km and deformation potentially related to deeper magma movement associated with the Altiplano-Puna

© 2023. The Authors.

This is an open access article under the terms of the [Creative Commons Attribution License](https://creativecommons.org/licenses/by/4.0/), which permits use, distribution and reproduction in any medium, provided the original work is properly cited.

Magma Body (APMB, Ward et al., 2014). The deformation signal near Cerro Overo, which has no ground-based monitoring, is intriguing as it transitioned from subsidence to uplift in ~2003–2005, which involves fluid accumulation and loss within the crust at ~10 km depth (Henderson & Pritchard, 2013). The deformation pattern of uplift at Lazufre (Lastarria and Azufre) has been interpreted to represent magma accumulation in the mid-upper crust with source depth <10 km (Díaz et al., 2015; Henderson et al., 2017; Pearse & Lundgren, 2013; Remy et al., 2014; Ruch & Walter, 2010), in addition to a source ~1 km under the Lastarria summit observed between 2003 and 2005 (Froger et al., 2007). Other deformation, for example, during the 2010 unrest at Lascar (which erupted in 2015–2017 without deformation, Gaete et al., 2020, and most recently in December 2022) can be linked to crater evolution processes such as gravitational slumping or piston-like subsidence (Richter et al., 2018). Putana and Sillajhuay showed short-lived, low-magnitude uplift in 2009 and 2007–2010, respectively, related to hydrothermal or seismic activity (Henderson & Pritchard, 2013; Pritchard et al., 2014; Stebel et al., 2014).

The triggers for episodes of magmatic uplift (or subsidence) in the Central Andes are obscure but could potentially include (a) variations in flux from lower crustal bodies of melt (e.g., the APMB) or (b) changes within shallow reservoirs such as crystal mush degassing as inferred in other settings (Pritchard et al., 2019). These processes cause pressure changes within reservoirs, thus controlling the initiation and cessation of inflation and deflation (or even possible episodic inflation and deflation as shown at Cerro Overo and Uturuncu, Walter & Motagh, 2014). The initiation of deformation may be linked to external events like earthquakes. For example, large subduction earthquakes in the Southern Andes and Japan caused stress field changes that triggered episodes of subsidence at multiple volcanoes (Pritchard et al., 2013; Takada & Fukushima, 2013), and regional earthquakes are also thought to have triggered delayed uplift through surface waves (e.g., Lupi et al., 2017).

Here, we analyze ~4 years of Sentinel-1 InSAR time series data, spanning January 2018 to October 2021, in the region of Antofagasta, Chile (Figure 1). Similarly to those previously reported, we observe uplift at Uturuncu, and Cerro Overo, and Azufre. However, we also find a previously unreported deformation signal centered on the Socompa volcano, where no deformation has previously been observed from regional InSAR studies (1992–2010, Henderson & Pritchard, 2013). We measure a steady linear uplift (rate of 17.5 ± 3.7 mm/yr) starting from November 2019, which continues through the rest of our InSAR observation time (until October 2021).

Socompa is a large stratovolcano (peak elevation 6,031 m) and is the site of a trainline and manned border control between Chile and Argentina. It is known for the failure of the northwestern flank that produced a 600 km² debris-avalanche deposit and triggered post-collapse eruptions ~7, 200 years ago (Wadge et al., 1995). As a result of its remote location and presumed quiescence, it lacks targeted ground monitoring, although it was selected as the site of a single Global Positioning System (GPS) station (ID: SOCM) installed in 2011 as part of the NSF PLUTONS network (Pritchard et al., 2018) due to its location halfway between Lazufre and Uturuncu and previously used as a far-field non-deforming reference station. A small lake at the foot, and several warmspots near the summit of the volcano form a complex microbial ecosystem (Costello et al., 2009; Farías et al., 2013; Halloy, 1991) where both water and CO₂ degassing have been observed during field studies (but not from a satellite IR survey; Jay et al., 2013), implying the presence of active hydrothermal and therefore magmatic systems.

We determine the precise onset time of uplift at Socompa using a time-dependent parameterized model fitting the GPS time series from SOCM, and investigate the temporal relationship between the onset of Socompa uplift and nearby earthquakes to explore the potential trigger mechanisms. We reconstruct the cumulative deformation fields using an InSAR time series approach (Liu et al., 2021), and combine both InSAR and GPS data as inputs to assess several potential geodetic source models to explain the Socompa deformation. Finally, we discuss the sudden onset of uplift at Socompa in the context of the long timescales of unrest as observed with InSAR in the Central Andean volcanoes since the 1990s.

2. InSAR Time Series Analysis

Here we process Sentinel-1 InSAR time series using the LiCSAR processing chain (Lazecký et al., 2020) and StaMPS software (Hooper et al., 2007, processing details in Text S1 in Supporting Information S1). Compared to single interferograms, InSAR time series analysis provides frequent estimates of surface displacement through time (every 6 or 12 days for Sentinel-1), reducing measurement uncertainties from noise (Osmanoğlu et al., 2016). In addition, if we assume a deformation model appropriate for displacements due to Socompa unrest, we can reconstruct the post-onset cumulative deformation field via a time-dependent parameterized model fitted to the

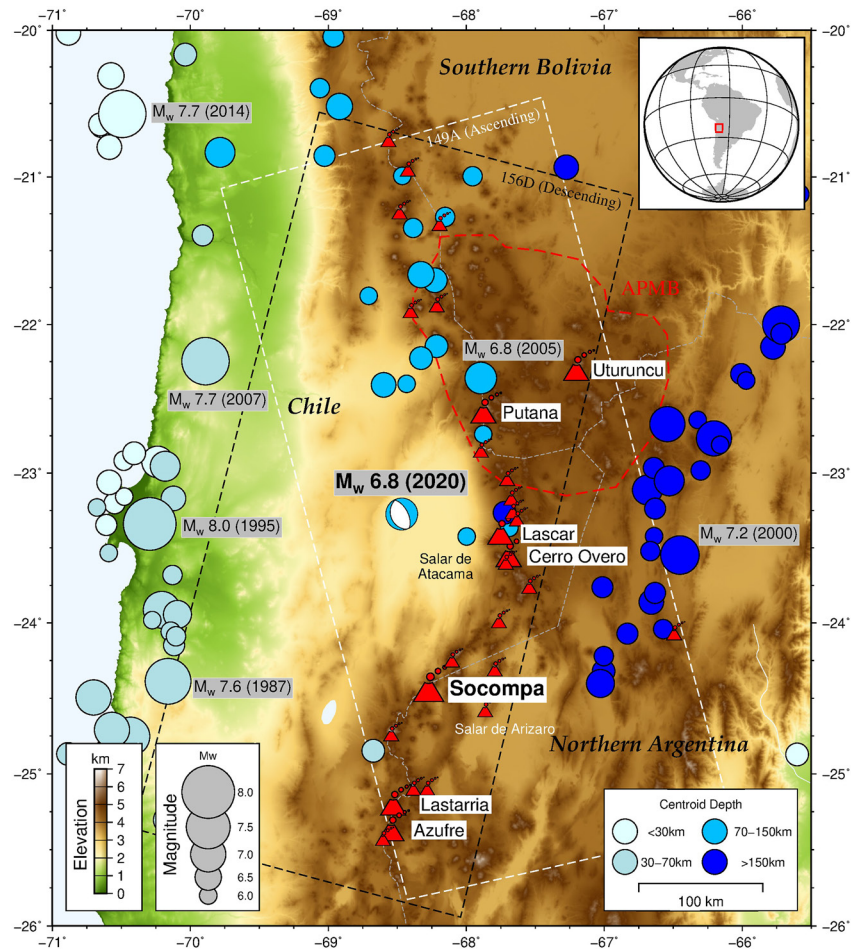


Figure 1. Topographic map of Northern Chile from Shuttle Radar Topography Mission (SRTM). White and black dashed rectangle boxes show the Sentinel-1 data coverage from two tracks (149A Ascending and 156D Descending, spanning January 2018 to October 2021). All Holocene volcanoes are marked and some active volcanoes with larger icons are labeled by their name. The red dashed line roughly defines the extent of the Altiplano-Puna Magma Body (Perkins et al., 2016). The M_w 6.8 earthquake epicenter (3 June 2020 with a 112 km centroid depth), is marked by the focal mechanism, while all the $M_w > 6.0$ historical earthquakes since 1976 (where a precise global seismic network was established) in this region are shown by blue circles colored by centroid depth (records from the USGS, United States Geological Survey).

InSAR time series. As the observed velocity change at Socompa is approximately linear, we assume that surface displacement at time t following the onset time t_0 can be decomposed as follows:

$$\psi(t) = V_1 t + H(t - t_0) V_2 t + b \quad (1)$$

where $H(*)$ is a Heaviside step function, V_1 is the background long-term linear deformation rate, V_2 is the linear velocity change after the onset time, and b is a constant reference offset in observations. We do not fit the seasonal signals because the already-applied Generic Atmospheric Correction Online Service (GACOS, Yu et al., 2018) should suppress the seasonality, and it is also difficult to model it accurately considering the noise level within the InSAR data in this region (particularly from ionospheric delay, Liang et al., 2019). After fitting the data, we reconstruct the cumulative pre- and post-onset deformation field in the line of sight (LOS) direction via the difference between the points at both ends of the fitting lines (Figure 2).

As the Central Andes predominately lacks vegetation, coherence is very high, significantly lowering the impact of unwrapping errors and fading signals (Agram & Simons, 2015). The main InSAR error sources arise from atmospheric noise, including both tropospheric and ionospheric components. Although the applied GACOS corrections (Yu et al., 2018) improve the data quality (with average standard error reductions of 16.9% and 45.7% for ascending and descending interferograms, respectively, Figure S1 in Supporting Information S1), the

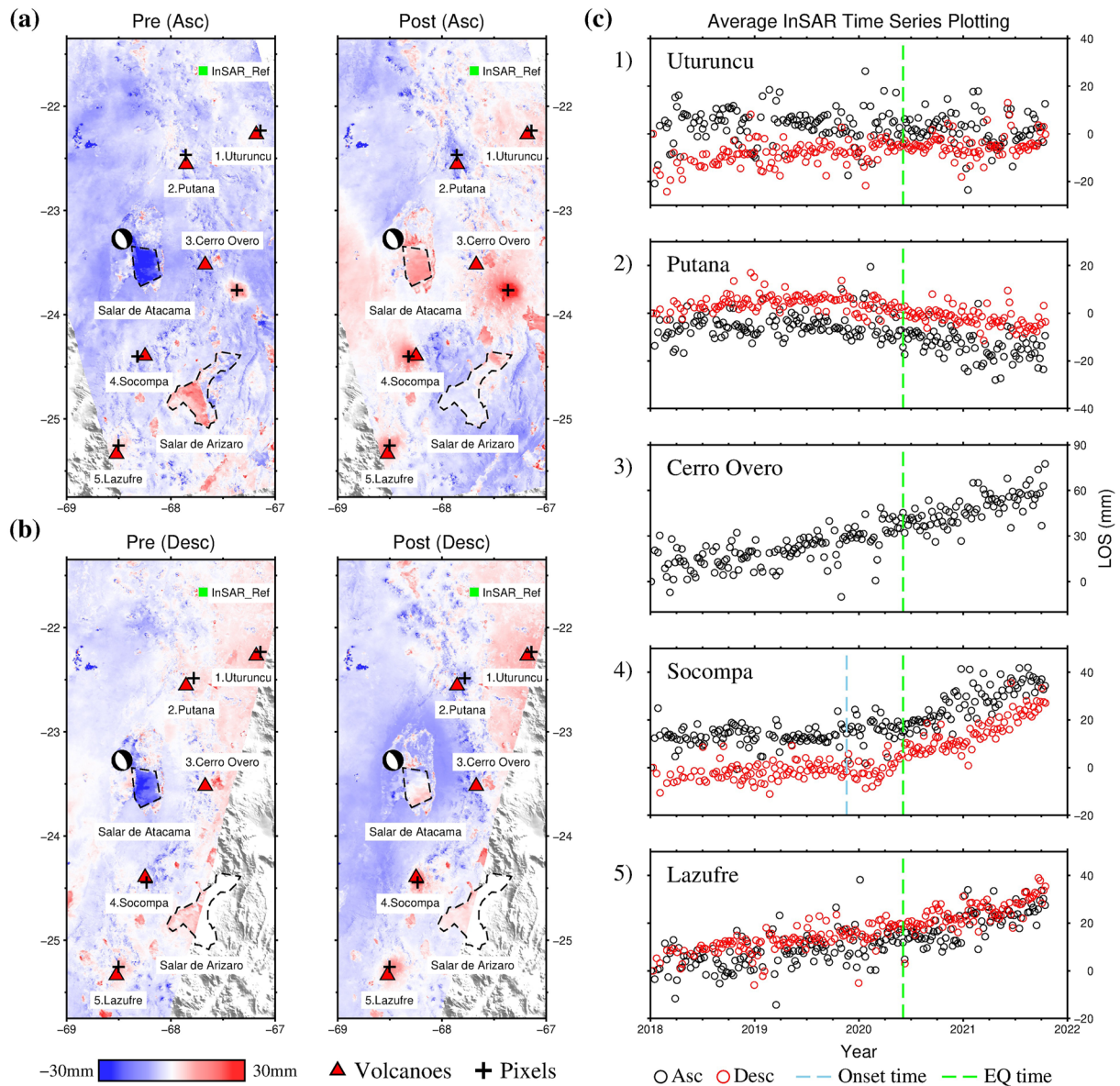


Figure 2. Reconstructed pre- and post-onset cumulative deformation fields and corresponding Interferometric Synthetic Aperture Radar (InSAR) time series plots. (a) The pre- and post-onset cumulative deformation fields using ascending track data. The focal mechanism, black dashed polygon, and green square represent the epicenter of the M_w 6.8 earthquake, the approximate boundaries of the salar (salt pan) regions (Text S2 in Supporting Information S1), and the InSAR reference points, respectively. The InSAR time series plots of some peak displacement pixels near the volcanoes are shown in (c). (b) Same as (a) but for descending track data. In all figures, positive values mean movement toward the satellite. Note the displacement signal associated with Cerro Overo is ~ 40 km southeast of the volcano and falls outside of the data coverage on the descending frame.

ionospheric noise is very strong and could not be ignored, especially on ascending track. We therefore remove a linear ramp that spans the whole interferogram to reduce ionospheric noise, and other long wavelength signals associated with orbit errors and plate motion. Overall, the noise level in the ascending data is much higher than for descending, and noticeable atmospheric artifacts remain in high topography areas.

3. Socompa Uplift

3.1. Onset Time Implications

Determining the onset time for Socompa uplift is important not only for reconstructing the cumulative deformation field, but also for investigating potential causes for initiating unrest at Socompa. Due to historically

lower temporal resolution satellite imagery and the typically long duration of unrest, it has not previously been possible to determine precisely the initiation time of deformation at a Central Andean volcano. For example, while uplift at Sabancaya is known to have started in 2013, the distribution of Synthetic Aperture Radar (SAR) acquisitions means that it could have taken place at any point over several months (Macqueen et al., 2020). Here we investigate potential triggering mechanisms from earthquakes in this region by exploring all major historical events ($M_w > 6.0$ since 1976, see Figure 1). We find the closest event in space and time is a M_w 6.8 intraslab earthquake with a 112 km centroid depth, which occurred on 3 June 2020, and whose epicenter is ~ 120 km northwest of Socompa (Figure S2 in Supporting Information S1). Initial visual inspection of the deformation signal pointed to the potential for a causal relationship given the close correlation in time, but the InSAR time series are noisy and contain seasonal signals that overprint changes in long-term trends.

3.2. Onset Time Determination

To determine the exact onset time, we collect data from a previously installed GPS station (SOCM, Henderson et al., 2017), which is located ~ 8 km southwest of the Socompa volcano and captures the deformation signal (Figure 3c). We use a time series with average daily positions processed by the Nevada Geodetic Laboratory in a South American Plate reference frame (Blewitt et al., 2018) to do a time-dependent parameterized fitting, using the trajectory model:

$$\begin{aligned} \delta(t) = & V_1 t + H(t - t_0) V_2 t + A_1 \sin(2\pi t + \varphi_1) \\ & + A_2 \sin(4\pi t + \varphi_2) + \sum H(t - t_{eq(i)}) C_i + b \end{aligned} \quad (2)$$

where the unit of time t is year, A_1 , A_2 and φ_1 , φ_2 are the amplitudes and phases of annual and semi-annual terms respectively, $t_{eq(i)}$ and C_i are historical earthquake event times and corresponding coseismic offsets that are close to the station (based on the database of the Nevada Geodetic Laboratory). We use a Markov Chain Monte Carlo approach to determine that the optimal onset time t_0 is 19 November 2019 (197 ± 12 days ahead of the earthquake event time, Text S3 in Supporting Information S1), using all three components of GPS time series data and weighting them by the noise level within each component (Figure 3a).

Such analysis highlights strong seasonal effects in the GPS time series, especially in the North direction, leaving some uncertainty about the onset time in the data fitting. To reduce the influence of seasonal signals, we further use a novel method of vector decomposition, transforming the East-North vectors into another orthogonal coordinate system, aligned along the movements parallel and perpendicular to the direction of seasonal motion (Text S4 in Supporting Information S1). The decomposition results (Figure 3b) clearly show an onset time half a year ahead of the earthquake, suggesting that unrest at Socompa was unlikely dynamically triggered by seismic waves induced by this earthquake.

3.3. Volcanic Geodetic Source Modeling

As we detect unrest at Socompa for the first time, we explore several source models to explain the observed deformation, including a point pressure source (Mogi, 1958), prolate spheroid (Yang et al., 1988), dipping dike with uniform opening (Okada, 1985), and a point Compound Dislocation Model (pCDM, Lundgren et al., 2017; Nikkhoo et al., 2017). We use the reconstructed post-onset cumulative deformation fields from the InSAR time series (November 2019 to October 2021), and cumulative GPS deformation at SOCM station that has the same time scale as InSAR data, as it improves the signal-to-noise ratio (SNR) of input data and subsequently provides more robust modeling results.

We first use a nested uniform downsampling of the reconstructed post-onset cumulative deformation fields, with a greater pixel density in the deformation area (Figure S3 in Supporting Information S1). Then we use the Geodetic Bayesian Inversion Software (GBIS, Bagnardi & Hooper, 2018), a Bayesian approach for the inversion of multiple geodetic data sets that provides the posterior probability density functions of source model parameters, to invert the model parameters. We embed the code of pCDM (Nikkhoo et al., 2017) into the GBIS software so that all models run in the same environment, and use the data uncertainty within the InSAR and GPS observations to weight them during the inversion (Figure S4 in Supporting Information S1).

To obtain the equivalent volume change of pCDM, we further use the point Ellipsoidal Cavity Model (pECM, Nikkhoo et al., 2017), a special case of pCDM i.e., constrained to represent a pressurized ellipsoidal cavity,

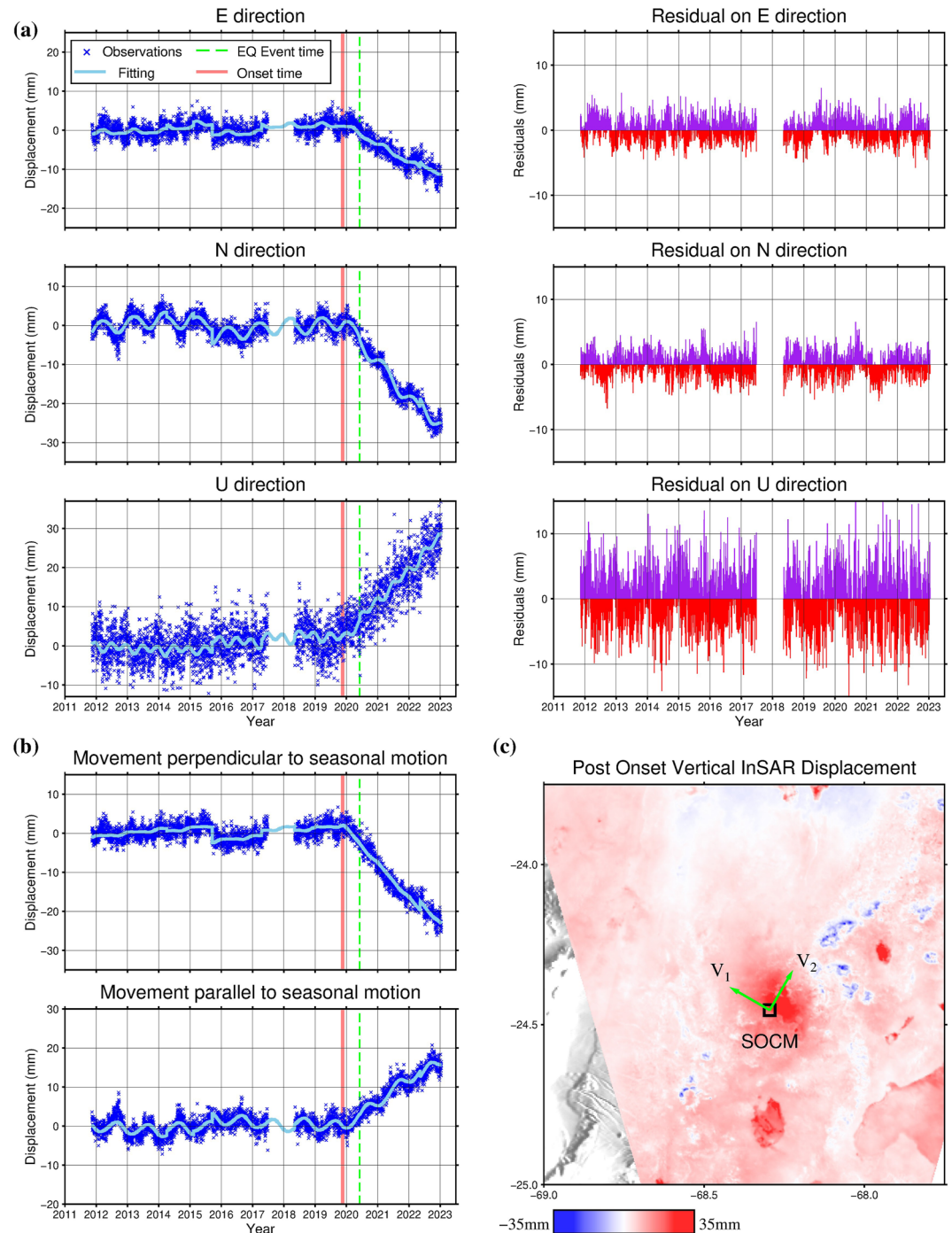


Figure 3. Global Positioning System (GPS) time series parameter fitting to determine the deformation onset at Socoma volcano. (a) Daily GPS time series and parameterized fitting using Equation 2, and corresponding residuals. The thick red vertical line shows the 95% confidence interval of the onset time. The data have been detrended using the Median Interannual Difference Adjusted for Skewness algorithm before fitting (Blewitt et al., 2016). (b) Decomposition of East and North directions of GPS data into movement perpendicular and parallel to the direction of seasonal motion. (c) The relative location of this SOCM GPS station, using the vertical post onset time cumulative deformation field decomposed from ascending and descending as the background image. The green arrows indicate the rough direction of movement perpendicular (V_1) and parallel (V_2) to the seasonal motion used in (b).

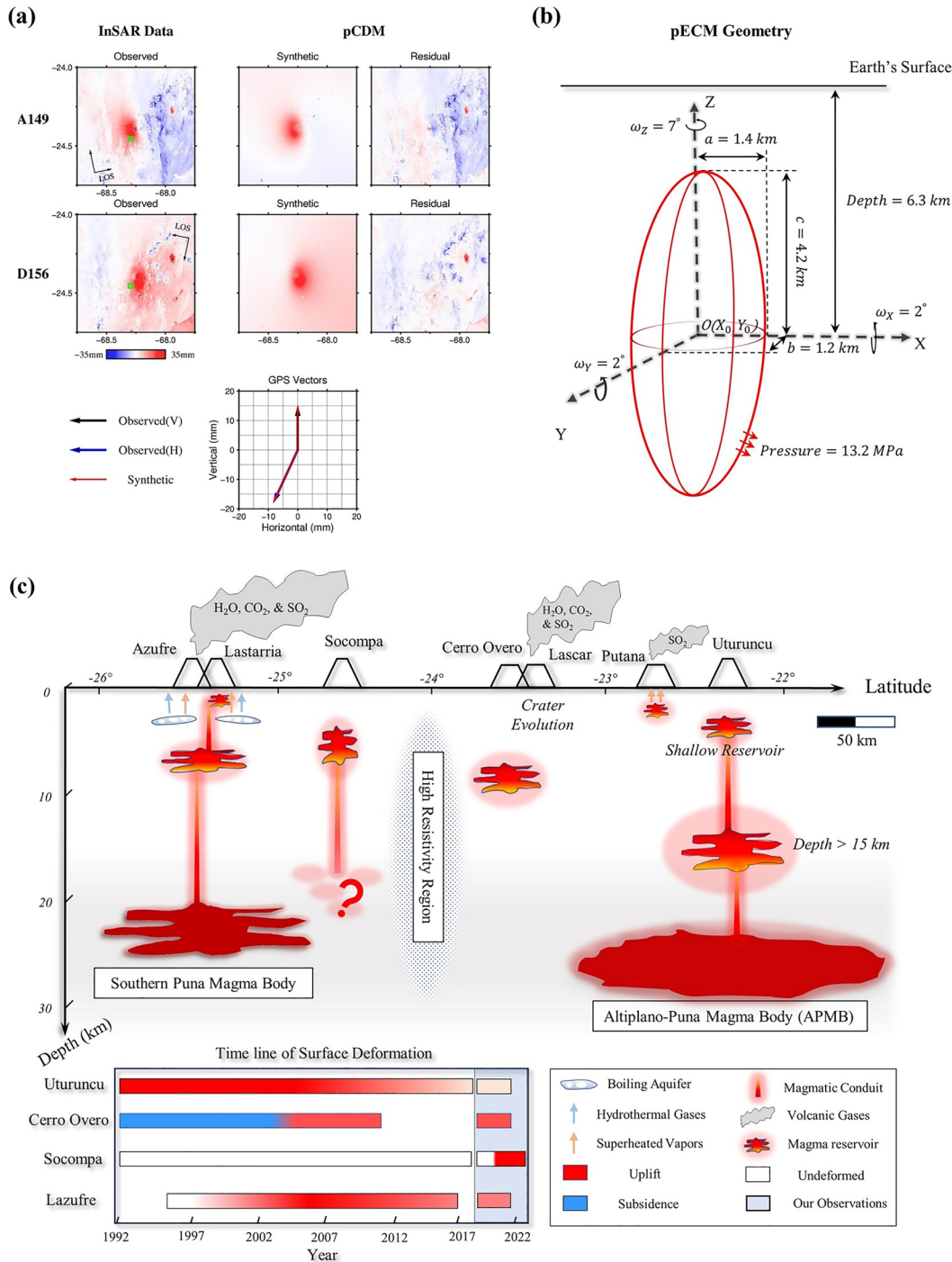


Figure 4.

to perform the inversion using the inferred source location and orientation from pCDM. Our modeling results show the Yang and pCDM (pECM) fits the observations best (Figure 4; Figures S5–S9 and Table S1 in Supporting Information S1, the values of reduced chi-squared, Text S5 in Supporting Information S1 are 0.42, 0.43, 0.48, and 0.65 for pCDM, Yang, Okada, and Mogi, respectively), and these two models give similar source depth (6.3 and 7.3 km for pCDM and Yang, respectively), geometry, and volume change ($\sim 1.1 \times 10^7 \text{ m}^3$ for both models).

4. Other Volcanic Deformations

Several volcanoes have been reported to be deforming in the past few decades (Figure 2) and we tie our InSAR observation to the GPS network in this region (Text S6 and Figure S10 in Supporting Information S1) to compare our results to these earlier studies. Starting in the north, Uturuncu previously showed a deformation rate of ~ 15 mm/yr in the 1990s (Fialko & Pearce, 2012; Henderson & Pritchard, 2013), but this gradually slowed in the 2010s (Gottsmann et al., 2017) to a rate of 3–5 mm/yr in ~ 2017 (Lau et al., 2018) and ~ 3 mm/yr in ~ 2020 (Eiden et al., 2023). In agreement with previous studies, we observe an uplift rate of 2.5 ± 1.8 mm/yr on Uturuncu (2018–2021, Figure S11a in Supporting Information S1). Putana displayed short-lived uplift totaling 40 mm displacement in 2009–2010 (Henderson & Pritchard, 2013), whilst we find potential subsidence of -3.9 ± 2.1 mm/yr (November 2019 to October 2021), with an onset which seems coincident with the deformation at Socompa (Figure S11b in Supporting Information S1). The deformation signal close to the Cerro Overo, which previously changed from subsidence of -4 mm/yr (1992–2003) to uplift of 5 mm/yr through 2010 on descending track (Henderson & Pritchard, 2013), continues to uplift at a rate of 3.8 ± 2.6 mm/yr (ascending LOS velocity, 2018–2021). Lazufre volcano shows uplift rates of 11.2 ± 1.7 mm/yr (2018–2021, Figure S11c in Supporting Information S1), consistent with the trend of surface deformation slowing at this volcano (Henderson et al., 2017; Henderson & Pritchard, 2013; Remy et al., 2014).

5. Discussion

Since uplift at Socompa started months before the M_w 6.8 intraslab earthquake, we instead consider a plausible explanation for the sudden uplift to be the ascent of magmatic fluids from a deeper melt source into a shallower reservoir. A magnetotelluric study (Ślęzak et al., 2021) in the Atacama region found a high conductivity zone at Socompa (~ 5 km west of the volcano and spanning 2 km to over 30 km depth), although there is significant uncertainty on the existence of the high conductivity zone as it is constrained by only one measurement point at Socompa, whereas the high resistivity region suggests that Socompa is unlikely connected to APMB (Figure 4c). The crust beneath Socompa and Cerro Overo has not been subject to the same level of study as Uturuncu and the APMB (e.g., Comeau et al., 2016). Deformation at Socompa has some first order similarities to that at Lazufre (~ 90 km to the South): they have similar source depth (< 10 km) and rate of volume change in order of 10^6 m³/yr (Henderson et al., 2017; Remy et al., 2014). The shallow reservoir and hydrothermal system beneath Lazufre have been suggested to be linked to the Southern Puna Magma Body (Budach et al., 2013; Stechern et al., 2017; Ward et al., 2017), but there is no independent evidence for this at Socompa.

An interesting question here is whether the initiation of uplift at Socompa will maintain a linear rate, decrease exponentially like at Lazufre or whether it will gradually slow and eventually cease. The current geodetic observations show no trace of deceleration, which in a purely elastic system would imply a constant pressure increase. Alternatively, it may be too early to detect any decrease in magnitude of a hydraulic connection to a deeper magma supply. Note that the current pressure we obtain from the model is ~ 13.2 MPa, which is far less than the overpressure required for chamber wall failure (Gerbault et al., 2018).

Deformation at Socompa is very consistent with other observations of unrest in the Central Andes (e.g., Henderson & Pritchard, 2013; Pritchard & Simons, 2004a). The deformation rate is low (usually < 30 mm/yr), and uplift started after an apparently very long period of quiescence (like Lazufre), consistent with deformation taking place on much longer timescales than other parts of the Andes (inter-eruptive and co-eruptive deformation rates are much higher in both the Northern and Southern Andes, e.g., Pritchard & Simons, 2004b; Fournier et al., 2010;

Figure 4. (a) Volcanic source model of Socompa cumulative uplift (November 2019 to October 2021) using point Compound Dislocation Model. It shows the modeling results of Interferometric Synthetic Aperture Radar (InSAR) and Global Positioning System (GPS) observations. The green box in InSAR observations indicates the location of the SOCM station. In the GPS panel, the black vertical vector represents the up-component deformation (~ 15 mm), while the blue vector signifies the horizontal deformation in the east (~ -10 mm) and north (~ -20 mm) directions. (b) Source geometry derived from point Ellipsoidal Cavity Model, which is defined by the source location (X_0, Y_0, Depth), the rotation angles around three axes ($\omega_x, \omega_y, \omega_z$), the semi-axes along three axes (a, b, c), and the pressure on the cavity walls. Poisson's ratio is 0.25 and shear modulus is 32 GPa here. (c) Cartoon depicting the magmatic systems in this region (approximate representation of relative locations), and those timelines of surface deformations from 1992 to 2023 measured by InSAR and GPS. Note the source depths vary based on different models and observation periods (e.g., Uturuncu 15–30 km, Lazufre < 10 km), and here we only plot the approximate depth of the magma reservoir, including the shallow reservoirs reported at Lastarria and Uturuncu (Froger et al., 2007; Gottsmann et al., 2022; Lau et al., 2018). We plot the rough depth of the Southern Puna Magma Body under Lazufre from Stechern et al., 2017, the shape and depth of Altiplano-Puna Magma Body from Ward et al., 2014, and the extent of the high resistivity region from Ślęzak et al., 2021. Depth at 0 km means the earth's surface at the local topography (summit elevations: 5,706 m at Lazufre, 6,031 m at Socompa, $\sim 5,000$ m at Cerro Overo, and 6,008 m at Uturuncu).

Morales Rivera et al., 2016). This means that Holocene activity is not necessarily a good basis for assessing whether Central Andean volcanoes have active magmatic systems or are likely to enter a phase of unrest. InSAR measurements of deformation are therefore critical for the detection of volcanic unrest. However, volcano deformation in the Central Andes is generally not associated with eruption (except at Sabancaya and Lascar), reflecting lower rates of reservoir pressurization and therefore lower rates of magma flux that are more conducive to intrusion growth than brittle failure, dyke propagation and magma ascent (Biggs & Pritchard, 2017).

6. Conclusion

Our observations update the volcanic monitoring at Central Andean volcanoes in Northern Chile. We first detected unrest at Socompa volcano, contribute to a picture of low-rate, episodic deformation in this region, indicative of magmatic processes that take place on very long time scales of decades. We determine the onset time of Socompa uplift in November 2019, with a linear rate of 17.5 mm/yr up to January 2023, using InSAR and GPS observations. We test several geodetic source models, finding the best-fit for an ellipsoidal source located at a depth of ~ 6.3 km and volume change of $\sim 6.2 \times 10^6$ m³/yr. We capture the onset of deformation at a Central Andean volcano for the first time at high temporal resolution, which suggests earthquake triggering is unlikely in this case. This provides a potentially important dataset for assessing the temporal development and therefore origin of such deformation.

Data Availability Statement

The Sentinel-1 SAR data are copyrighted by the European Space Agency and additionally distributed by the Alaska Satellite Facility Distributed Active Archive Center (<https://earthdata.nasa.gov/eosdis/daacs/asf>). All the GPS data we use, including SOCM (<https://www.unavco.org/data/doi/10.7283/T5TT4P27>), is processed by the Nevada Geodetic Laboratory (<http://geodesy.unr.edu>), which are based on services provided by the GAGE Facility, operated by UNAVCO, Inc., with support from the National Science Foundation, the National Aeronautics and Space Administration, and the U.S. Geological Survey under NSF Cooperative Agreement EAR-1724794. The InSAR time series fitting and geodetic modelling results are available on Zenodo (<https://doi.org/10.5281/zenodo.7688945>).

References

- Agram, P. S., & Simons, M. (2015). A noise model for InSAR time series. *Journal of Geophysical Research: Solid Earth*, 120(4), 2752–2771. <https://doi.org/10.1002/2014JB011271>
- Aguilera, F., Apaza, F., Del Carpio, J., Grosse, P., Jiménez, N., Ureta, G., et al. (2022). Advances in scientific understanding of the Central Volcanic Zone of the Andes: A review of contributing factors. *Bulletin of Volcanology*, 84(3), 22. <https://doi.org/10.1007/s00445-022-01526-y>
- Bagnardi, M., & Hooper, A. (2018). Inversion of surface deformation data for rapid estimates of source parameters and uncertainties: A Bayesian approach. *Geochemistry, Geophysics, Geosystems*, 19(7), 2194–2211. <https://doi.org/10.1029/2018GC007585>
- Barone, A., Fedi, M., Tizzani, P., & Castaldo, R. (2019). Multiscale analysis of DInSAR measurements for multi-source investigation at Uturuncu volcano (Bolivia). *Remote Sensing*, 11(6), 703. <https://doi.org/10.3390/rs11060703>
- Biggs, J., Ebmeier, S. K., Aspinall, W. P., Lu, Z., Pritchard, M. E., Sparks, R. S. J., & Mather, T. A. (2014). Global link between deformation and volcanic eruption quantified by satellite imagery. *Nature Communications*, 5(1), 3471. <https://doi.org/10.1038/ncomms4471>
- Biggs, J., & Pritchard, M. E. (2017). Global volcano monitoring: What does it mean when volcanoes deform? *Elements*, 13(1), 17–22. <https://doi.org/10.2113/gselements.13.1.17>
- Blewitt, G., Hammond, W. C., & Kreemer, C. (2018). Harnessing the GPS data explosion for interdisciplinary science. *Eos*, 99. <https://doi.org/10.1029/2018EO104623>
- Blewitt, G., Kreemer, C., Hammond, W. C., & Gazeaux, J. (2016). MIDAS robust trend estimator for accurate GPS station velocities without step detection. *Journal of Geophysical Research: Solid Earth*, 121(3), 2054–2068. <https://doi.org/10.1002/2015JB012552>
- Budach, I., Brasse, H., & Díaz, D. (2013). Crustal-scale electrical conductivity anomaly beneath inflating Lazufre volcanic complex, Central Andes. *Journal of South American Earth Sciences*, 42, 144–149. <https://doi.org/10.1016/j.jsames.2012.11.002>
- Chaussard, E., & Amelung, F. (2012). Precursory inflation of shallow magma reservoirs at west Sunda volcanoes detected by InSAR. *Geophysical Research Letters*, 39(21), 6–11. <https://doi.org/10.1029/2012GL053817>
- Comeau, M. J., Unsworth, M. J., & Cordell, D. (2016). New constraints on the magma distribution and composition beneath Volcán Uturuncu and the southern Bolivian Altiplano from magnetotelluric data. *Geosphere*, 12(5), 1391–1421. <https://doi.org/10.1130/GES01277.1>
- Costello, E. K., Halloy, S. R. P., Reed, S. C., Sowell, P., & Schmidt, S. K. (2009). Fumarole-supported islands of biodiversity within a hyper-arid, high-elevation landscape on Socompa Volcano, Puna de Atacama, Andes. *Applied and Environmental Microbiology*, 75(3), 735–747. <https://doi.org/10.1128/AEM.01469-08>
- Díaz, D., Heise, W., & Zamudio, F. (2015). Three-dimensional resistivity image of the magmatic system beneath Lastarria volcano and evidence for magmatic intrusion in the back arc (northern Chile). *Geophysical Research Letters*, 42(13), 5212–5218. <https://doi.org/10.1002/2015GL064426>
- Ebmeier, S. K., Andrews, B. J., Araya, M. C., Arnold, D. W. D., Biggs, J., Cooper, C., et al. (2018). Synthesis of global satellite observations of magmatic and volcanic deformation: Implications for volcano monitoring & the lateral extent of magmatic domains. *Journal of Applied Volcanology*, 7(1), 1–26. <https://doi.org/10.1186/s13617-018-0071-3>

Acknowledgments

This work is supported by the UK Natural Environment Research Council (NERC) through the Centre for the Observation and Modelling of Earthquakes, Volcanoes and Tectonics (COMET, <http://comet.nerc.ac.uk>), and the Looking into the Continents from Space (LiCS) large Grant (NE/K010867/1). Figures were made using the Generic Mapping Tools (GMT) (Wessel et al., 2013). FL acknowledges support from the Great Britain-China Educational Trust. JE and TC acknowledge support from the Royal Society through University Research Fellowships (UF150282 and URF1180088). SE is funded by a NERC Independent Research Fellowship (NE/R015546/1). AH and CNL acknowledge support from the European Research Council (ERC) through the EU Horizon 2020 project DEEPVOLC (Grant 866085). FD thanks FONDECYT Iniciación 11220513 research grant for funding. We acknowledge Kristina Butler, Catherine Gagnon, Joaquín Castillo, Sofia Parra, Milton Quinteros, and Gabriela Herrera for collecting the GPS data of the SOCM station. We thank Scott Henderson, Julie Elliott, and especially Matthew Pritchard (for installing the SOCM station) for their help in retrieving and processing the data.

- Eiden, E., MacQueen, P., Henderson, S., & Pritchard, M. (2023). Multiple spatial and temporal scales of deformation from geodetic monitoring point to active transcrustal magma system at Uturuncu volcano. *Bolivia*, 19(2), 370–382. <https://doi.org/10.1130/GES02520.1>
- Fariás, M. E., Rascovan, N., Toneatti, D. M., Albarracín, V. H., Flores, M. R., Poiré, D. G., et al. (2013). The discovery of stromatolites developing at 3570 m above sea level in a high-altitude volcanic lake Socompa, Argentinean Andes. *PLoS One*, 8(1), e53497. <https://doi.org/10.1371/journal.pone.0053497>
- Fialko, Y., & Pearse, J. (2012). Sombrero uplift above the Altiplano-Puna magma body: Evidence of a ballooning mid-crustal diapir. *Science*, 338(6104), 250–252. <https://doi.org/10.1126/science.1226358>
- Fournier, T. J., Pritchard, M. E., & Riddick, S. N. (2010). Duration, magnitude, and frequency of subaerial volcano deformation events: New results from Latin America using InSAR and a global synthesis. *Geochemistry, Geophysics, Geosystems*, 11(1). <https://doi.org/10.1029/2009GC002558>
- Froger, J. L., Remy, D., Bonvalot, S., & Legrand, D. (2007). Two scales of inflation at Lastarria-Cordon del Azufre volcanic complex, Central Andes, revealed from ASAR-ENVISAT interferometric data. *Earth and Planetary Science Letters*, 255(1–2), 148–163. <https://doi.org/10.1016/j.epsl.2006.12.012>
- Gaete, A., Walter, T. R., Bredemeyer, S., Zimmer, M., Kujawa, C., Franco Marin, L., et al. (2020). Processes culminating in the 2015 phreatic explosion at Lascar volcano, Chile, evidenced by multiparametric data. *Natural Hazards and Earth System Sciences*, 20(2), 377–397. <https://doi.org/10.5194/nhess-20-377-2020>
- Gerbault, M., Hassani, R., Novoa Lizama, C., & Souche, A. (2018). Three-dimensional failure patterns around an inflating magmatic chamber. *Geochemistry, Geophysics, Geosystems*, 19(3), 749–771. <https://doi.org/10.1002/2017GC007174>
- Gottsmann, J., Blundy, J., Henderson, S., Pritchard, M. E., & Sparks, R. S. J. (2017). Thermomechanical modeling of the Altiplano-Puna deformation anomaly: Multiparameter insights into magma mush reorganization. *Geosphere*, 13(4), 1042–1065. <https://doi.org/10.1130/GES01420.1>
- Gottsmann, J., Eiden, E., & Pritchard, M. E. (2022). Transcrustal compressible fluid flow explains the Altiplano-Puna gravity and deformation anomalies. *Geophysical Research Letters*, 49(16), e2022GL099487. <https://doi.org/10.1029/2022GL099487>
- Halloy, S. (1991). Islands of life at 6000 m altitude: The environment of the highest autotrophic communities on Earth (Socompa Volcano, Andes). *Arctic and Alpine Research*, 23(3), 247–262. <https://doi.org/10.1080/00040851.1991.12002843>
- Henderson, S. T., Delgado, F., Elliott, J., Pritchard, M. E., & Lundgren, P. R. (2017). Decelerating uplift at Lafuzre volcanic center, Central Andes, from A.D. 2010 to 2016, and implications for geodetic models. *Geosphere*, 13(5), 1489–1505. <https://doi.org/10.1130/GES01441.1>
- Henderson, S. T., & Pritchard, M. E. (2013). Decadal volcanic deformation in the Central Andes volcanic zone revealed by InSAR time series. *Geochemistry, Geophysics, Geosystems*, 14(5), 1358–1374. <https://doi.org/10.1002/ggge.20074>
- Henderson, S. T., & Pritchard, M. E. (2017). Time-dependent deformation of Uturuncu volcano, Bolivia, constrained by GPS and InSAR measurements and implications for source models. *Geosphere*, 13(6), 1834–1854. <https://doi.org/10.1130/GES01203.1>
- Hickey, J., Gottsmann, J., & Del Potro, R. (2013). The large-scale surface uplift in the Altiplano-Puna region of Bolivia: A parametric study of source characteristics and crustal rheology using finite element analysis. *Geochemistry, Geophysics, Geosystems*, 14(3), 540–555. <https://doi.org/10.1002/ggge.20057>
- Hooper, A., Segall, P., & Zebker, H. (2007). Persistent scatterer interferometric synthetic aperture radar for crustal deformation analysis, with application to Volcán Alcedo, Galápagos. *Journal of Geophysical Research*, 112, B07407. <https://doi.org/10.1029/2006JB004763>
- Jay, J. A., Welch, M., Pritchard, M. E., Mares, P. J., Mnich, M. E., Melkonian, A. K., et al. (2013). Volcanic hotspots of the central and southern Andes as seen from space by ASTER and MODVOLC between the years 2000 and 2010. *Geological Society Special Publication*, 380(1), 161–185. <https://doi.org/10.1144/SP380.1>
- Lau, N., Tymofeyeva, E., & Fialko, Y. (2018). Variations in the long-term uplift rate due to the Altiplano-Puna magma body observed with Sentinel-1 interferometry. *Earth and Planetary Science Letters*, 491, 43–47. <https://doi.org/10.1016/j.epsl.2018.03.026>
- Lazecký, M., Spaans, K., González, P. J., Maghsoudi, Y., Morishita, Y., Albino, F., et al. (2020). LiCSAR: An automatic InSAR tool for measuring and monitoring tectonic and volcanic activity. *Remote Sensing*, 12(15), 2430. <https://doi.org/10.3390/RS12152430>
- Liang, C., Agram, P., Simons, M., & Fielding, E. J. (2019). Ionospheric correction of InSAR time series analysis of C-band sentinel-1 TOPS data. *IEEE Transactions on Geoscience and Remote Sensing*, 57(9), 6755–6773. <https://doi.org/10.1109/TGRS.2019.2908494>
- Liu, F., Elliott, J. R., Craig, T. J., Hooper, A., & Wright, T. J. (2021). Improving the resolving power of InSAR for earthquakes using time series: A case study in Iran. *Geophysical Research Letters*, 48, e2021GL093043. <https://doi.org/10.1029/2021GL093043>
- Lundgren, P., Nikkhoo, M., Samsonov, S. V., Milillo, P., Gil-Cruz, F., & Lazo, J. (2017). Source model for the Copahue volcano magma plumbing system constrained by InSAR surface deformation observations. *Journal of Geophysical Research: Solid Earth*, 122(7), 5729–5747. <https://doi.org/10.1002/2017JB014368>
- Lupi, M., Frehner, M., Weis, P., Skelton, A., Saenger, E. H., Tisato, N., et al. (2017). Regional earthquakes followed by delayed ground uplifts at Campi Flegrei Caldera, Italy: Arguments for a causal link. *Earth and Planetary Science Letters*, 474, 436–446. <https://doi.org/10.1016/j.epsl.2017.07.006>
- MacQueen, P., Delgado, F., Reath, K., Pritchard, M. E., Bagnardi, M., Milillo, P., et al. (2020). Volcano-tectonic interactions at Sabancaya volcano, Peru: Eruptions, magmatic inflation, moderate earthquakes, and fault creep. *Journal of Geophysical Research: Solid Earth*, 125, e2019JB019281. <https://doi.org/10.1029/2019JB019281>
- Mogi, K. (1958). Relations between the eruptions of various volcanoes and the deformations of the ground surfaces around them. *Bulletin of Earthquake Research Institute*, 36, 99–134.
- Morales Rivera, A. M., Amelung, F., & Mothes, P. (2016). Volcano deformation survey over the Northern and Central Andes with ALOS InSAR time series. *Geochemistry, Geophysics, Geosystems*, 17(7), 2869–2883. <https://doi.org/10.1002/2016GC006393>
- Nikkhoo, M., Walter, T. R., Lundgren, P. R., & Prats-Iraola, P. (2017). Compound dislocation models (CDMs) for volcano deformation analyses. *Geophysical Journal International*, 208(2), 877–894. <https://doi.org/10.1093/gji/ggw427>
- Okada, Y. (1985). Surface deformation due to shear and tensile faults in a half-space. *Bulletin of the Seismological Society of America*, 75(4), 1135–1154. <https://doi.org/10.1785/BSSA0750041135>
- Osmanoğlu, B., Sunar, F., Wdowski, S., & Cabral-Cano, E. (2016). Time series analysis of InSAR data: Methods and trends. *ISPRS Journal of Photogrammetry and Remote Sensing*, 115, 90–102. <https://doi.org/10.1016/j.isprsjprs.2015.10.003>
- Pearse, J., & Lundgren, P. (2013). Source model of deformation at Lafuzre volcanic center, Central Andes, constrained by InSAR time series. *Geophysical Research Letters*, 40(6), 1059–1064. <https://doi.org/10.1002/grl.50276>
- Perkins, J. P., Ward, K. M., de Silva, S. L., Zandt, G., Beck, S. L., & Finnegan, N. J. (2016). Surface uplift in the Central Andes driven by growth of the Altiplano Puna Magma Body. *Nature Communications*, 7(1), 13185. <https://doi.org/10.1038/ncomms13185>
- Poland, M. P., & Zebker, H. A. (2022). Volcano geodesy using InSAR in 2020: The past and next decades. *Bulletin of Volcanology*, 84(3), 27. <https://doi.org/10.1007/s00445-022-01531-1>
- Pritchard, M. E., de Silva, S. L., Michelfelder, G., Zandt, G., McNutt, S. R., Gottsmann, J., et al. (2018). Synthesis: PLUTONS: Investigating the relationship between pluton growth and volcanism in the Central Andes. *Geosphere*, 14(3), 954–982. <https://doi.org/10.1130/GES01578.1>

- Pritchard, M. E., Henderson, S. T., Jay, J. A., Soler, V., Krzesni, D. A., Button, N. E., et al. (2014). Reconnaissance earthquake studies at nine volcanic areas of the Central Andes with coincident satellite thermal and InSAR observations. *Journal of Volcanology and Geothermal Research*, 280, 90–103. <https://doi.org/10.1016/j.jvolgeores.2014.05.004>
- Pritchard, M. E., Jay, J. A., Aron, F., Henderson, S. T., & Lara, L. E. (2013). Subsidence at southern Andes volcanoes induced by the 2010 Maule, Chile earthquake. *Nature Geoscience*, 6(8), 632–636. <https://doi.org/10.1038/ngeo1855>
- Pritchard, M. E., Mather, T. A., McNutt, S. R., Delgado, F. J., & Reath, K. (2019). Thoughts on the criteria to determine the origin of volcanic unrest as magmatic or non-magmatic. *Philosophical Transactions of the Royal Society A*, 377(2139), 20180008. <https://doi.org/10.1098/rsta.2018.0008>
- Pritchard, M. E., & Simons, M. (2002). A satellite geodetic survey of large-scale deformation of volcanic centres in the Central Andes. *Nature*, 418(6894), 167–171. <https://doi.org/10.1038/nature00872>
- Pritchard, M. E., & Simons, M. (2004a). An InSAR-based survey of volcanic deformation in the Central Andes. *Geochemistry, Geophysics, Geosystems*, 5(2), Q02002. <https://doi.org/10.1029/2003GC000610>
- Pritchard, M. E., & Simons, M. (2004b). An InSAR-based survey of volcanic deformation in the southern Andes. *Geophysical Research Letters*, 31, L15610. <https://doi.org/10.1029/2004GL020545>
- Reath, K., Pritchard, M., Poland, M., Delgado, F., Carn, S., Coppola, D., et al. (2019). Thermal, deformation, and degassing remote sensing time series (CE 2000–2017) at the 47 most active volcanoes in Latin America: Implications for volcanic systems. *Journal of Geophysical Research: Solid Earth*, 124(1), 195–218. <https://doi.org/10.1029/2018JB016199>
- Remy, D., Froger, J. L., Perfettini, H., Bonvalot, S., Gabalda, G., Albino, F., et al. (2014). Persistent uplift of the Lazufre volcanic complex (Central Andes): New insights from PCAIM inversion of InSAR time series and GPS data. *Geochemistry, Geophysics, Geosystems*, 15(9), 3591–3611. <https://doi.org/10.1002/2014GC005370>
- Richter, N., Salzer, J. T., de Zeeuw-van Dalfsen, E., Perissin, D., & Walter, T. R. (2018). Constraints on the geomorphological evolution of the nested summit craters of Láscar volcano from high spatio-temporal resolution TerraSAR-X interferometry. *Bulletin of Volcanology*, 80(3), 21. <https://doi.org/10.1007/s00445-018-1195-3>
- Ruch, J., & Walter, T. R. (2010). Relationship between the InSAR-measured uplift, the structural framework, and the present-day stress field at Lazufre volcanic area, Central Andes. *Tectonophysics*, 492(1–4), 133–140. <https://doi.org/10.1016/j.tecto.2010.06.003>
- Ślęzak, K., Díaz, D., Vargas, J. A., Cordell, D., Reyes-Cordova, F., & Segovia, M. J. (2021). Magnetotelluric image of the Chilean subduction zone in the Salar de Atacama region (23°–24°S): Insights into factors controlling the distribution of volcanic arc magmatism. *Physics of the Earth and Planetary Interiors*, 318, 106765. <https://doi.org/10.1016/j.pepi.2021.106765>
- Stebel, K., Amigo, A., Thomas, H., & Prata, A. J. (2014). First estimates of fumarolic SO₂ fluxes from Putana volcano, Chile, using an ultraviolet imaging camera. *Journal of Volcanology and Geothermal Research*, 300, 112–120. <https://doi.org/10.1016/j.jvolgeores.2014.12.021>
- Stechern, A., Just, T., Holtz, F., Blume-Oeste, M., & Namur, O. (2017). Decoding magma plumbing and geochemical evolution beneath the Lastarria volcanic complex (Northern Chile)—Evidence for multiple magma storage regions. *Journal of Volcanology and Geothermal Research*, 338, 25–45. <https://doi.org/10.1016/j.jvolgeores.2017.03.018>
- Takada, Y., & Fukushima, Y. (2013). Volcanic subsidence triggered by the 2011 Tohoku earthquake in Japan. *Nature Geoscience*, 6(8), 637–641. <https://doi.org/10.1038/ngeo1857>
- Wadge, G., Francis, P. W., & Ramirez, C. F. (1995). The Socompa collapse and avalanche event. *Journal of Volcanology and Geothermal Research*, 66(1–4), 309–336. [https://doi.org/10.1016/0377-0273\(94\)00083-s](https://doi.org/10.1016/0377-0273(94)00083-s)
- Walter, T. R., & Motagh, M. (2014). Deflation and inflation of a large magma body beneath Uturuncu Volcano, Bolivia? Insights from InSAR data, surface lineaments and stress modelling. *Geophysical Journal International*, 198(1), 462–473. <https://doi.org/10.1093/gji/ggu080>
- Ward, K. M., Delph, J. R., Zandt, G., Beck, S. L., & Ducea, M. N. (2017). Magmatic evolution of a Cordilleran flare-up and its role in the creation of silicic crust. *Scientific Reports*, 7(1), 9047. <https://doi.org/10.1038/s41598-017-09015-5>
- Ward, K. M., Zandt, G., Beck, S. L., Christensen, D. H., & McFarlin, H. (2014). Seismic imaging of the magmatic underpinnings beneath the Altiplano-Puna volcanic complex from the joint inversion of surface wave dispersion and receiver functions. *Earth and Planetary Science Letters*, 404, 43–53. <https://doi.org/10.1016/j.epsl.2014.07.022>
- Wessel, P., Smith, W. H. F., Scharroo, R., Luis, J., & Wobbe, F. (2013). Generic mapping tools: Improved version released. *Eos*, 94(45), 409–410. <https://doi.org/10.1002/2013EO450001>
- Yang, X. M., Davis, P. M., & Dieterich, J. H. (1988). Deformation from inflation of a dipping finite prolate spheroid in an elastic half-space as a model for volcanic stressing. *Journal of Geophysical Research*, 93(B5), 4249–4257. <https://doi.org/10.1029/JB093iB05p04249>
- Yu, C., Li, Z., Penna, N. T., & Crippa, P. (2018). Generic atmospheric correction model for interferometric synthetic aperture radar observations. *Journal of Geophysical Research: Solid Earth*, 123(10), 9202–9222. <https://doi.org/10.1029/2017JB015305>
- Yunjun, Z., Amelung, F., & Aoki, Y. (2021). Imaging the hydrothermal system of Kirishima volcanic complex with L-band InSAR time series. *Geophysical Research Letters*, 48, e2021GL092879. <https://doi.org/10.1029/2021GL092879>

References From the Supporting Information

- Ansari, H., De Zan, F., & Parizzi, A. (2020). Study of systematic bias in measuring surface deformation with SAR interferometry. *IEEE Transactions on Geoscience and Remote Sensing*, December, 59(2), 1285–1301. <https://doi.org/10.1109/TGRS.2020.3003421>
- Bekaert, D. P. S., Walters, R. J., Wright, T. J., Hooper, A. J., & Parker, D. J. (2015). Statistical comparison of InSAR tropospheric correction techniques. *Remote Sensing of Environment*, 170, 40–47. <https://doi.org/10.1016/j.rse.2015.08.035>
- Hussain, E., Hooper, A., Wright, T. J., Walters, R. J., & Bekaert, D. P. S. (2016). Interseismic strain accumulation across the central North Anatolian Fault from iteratively unwrapped InSAR measurements. *Journal of Geophysical Research: Solid Earth*, 121(12), 9000–9019. <https://doi.org/10.1002/2016JB013108>
- Liu, W., Agusdinata, D. B., & Myint, S. W. (2019). Spatiotemporal patterns of lithium mining and environmental degradation in the Atacama Salt Flat, Chile. *International Journal of Applied Earth Observation and Geoinformation*, 80, 145–156. <https://doi.org/10.1016/j.jag.2019.04.016>
- Maghsoudi, Y., Hooper, A. J., Wright, T. J., Lazecky, M., & Ansari, H. (2022). Characterizing and correcting phase biases in short-term, multi-looked interferograms. *Remote Sensing of Environment*, 275, 113022. <https://doi.org/10.1016/j.rse.2022.113022>
- Pavez, A., Remy, D., Bonvalot, S., Diament, M., Gabalda, G., Froger, J. L., et al. (2006). Insight into ground deformations at Láscar volcano (Chile) from SAR interferometry, photogrammetry and GPS data: Implications on volcano dynamics and future space monitoring. *Remote Sensing of Environment*, 100(3), 307–320. <https://doi.org/10.1016/j.rse.2005.10.013>
- Pritchard, M. E. (2003). *Recent crustal deformation in west-central South America*. (Doctoral dissertation). California Institute of Technology. Retrieved from <https://resolver.caltech.edu/CaltechETD:etd-06022003-105512>

- Purcell, V., Reddin, E., Ebmeier, S., González, P. J., Watson, A., Morishita, Y., & Elliott, J. (2022). Nearly three centuries of lava flow subsidence at Timanfaya, Lanzarote. *Geochemistry, Geophysics, Geosystems*, 23, e2022GC010576. <https://doi.org/10.1029/2022gc010576>
- Ruch, J., Warren, J. K., Risacher, F., Walter, T. R., & Lanari, R. (2012). Salt lake deformation detected from space. *Earth and Planetary Science Letters*, 331–332, 120–127. <https://doi.org/10.1016/j.epsl.2012.03.009>
- Webster, R., & Oliver, M. A. (2007). *Geostatistics for environmental scientists* (2nd ed.). John Wiley & Sons. <https://doi.org/10.1002/9780470517277>